Title

Heavy element formation in compound nucleus reactions with 238U targets

Authors
Gregorich, K
Dullman, CE
Loveland, W
et al.

Publication Date
2023-12-07

Peer reviewed

Heavy element formation in compound nucleus reactions with ^{238}U targets

K.E. Gregorich,[1] Ch.E. Düllmann,[1,2,3] W. Loveland,[4] C.M. Folden III,[1,2,5] J.M. Gates,[1,2] M.A. Garcia,[1,2] R. Sudowe,[1,6] L. Stavsetra,[1] I. Dragojević,[1,2] S.L. Nelson,[1,2] G.K. Pang,[2,5] P. M. Zielinski,[1,2] Y.H. Chung,[7] R. Eichler,[8,9] M. Schädel,[3] A. Türler,[10] A. Yakushev,[10] J. Dvorak,[10] D.C. Hoffman,[1,2] H. Nitsche[1,2]

[1]*Nuclear Science Division, Lawrence Berkeley National Laboratory, Berkeley, California 94720*

[2]*Department of Chemistry, University of California, Berkeley, California 94720*

[3]*Bereich Schwere Elemente, Gesellschaft für Schwerionenforschung, 64291 Darmstadt, Germany*

[4]*Department of Chemistry, Oregon State University, Corvallis, Oregon 97331*

[5]*National Superconducting Cyclotron Laboratory, Michigan State University, East Lansing, MI 48824*

[6]*Department of Health Physics, University of Nevada Las Vegas, Las Vegas, NV 89154*

[7]*Department of Chemistry, Hallym University, Chuncheon, Korea 200-702*

[8]*Labor für Radio- und Umweltchemie, Paul Scherrer Institut, CH-5232 Villigen PSI, Switzerland*

[9]*Departement für Chemie und Biochemie, Universität Bern, CH-3012 Bern, Switzerland*

[10]*Institut für Radiochemie, Technische Universität München, 85748 Garching, Germany*

(22 Novenber 2007)

Cross sections for heavy element formation by compound-nucleus reactions have been measured for reactions with ^{22}Ne, ^{23}Na, ^{26}Mg, ^{27}Al, ^{30}Si, ^{31}P, and ^{37}Cl projectiles and ^{238}U targets. Together with previously published results for reactions of ^{18}O, ^{19}F, ^{34}S, ^{40}Ar, and ^{48}Ca projectiles with ^{238}U targets, the systematics of heavy element formation cross sections are analyzed. Conclusions about critical angular momentum for fusion and neutron evaporation in competition with fission during de-excitation are drawn.

PACS Number(s): 25.70.Gh, 27.90.+b

Isotopes of the heaviest elements ($Z \geq 100$) can be produced in compound nucleus – evaporation reactions. Several authors have noted an exponential decrease [1-3] in heavy element formation cross sections with increasing compound nucleus Z. Recent reports [2] of constant picobarn-level cross sections for formation of superheavy elements (SHE) in ^{48}Ca irradiations of actinide targets constitute a break in this well-established trend. There are now reports of two independent confirmations [4,5] of SHE production in such reactions. Understanding the heavy element formation cross section mechanism has taken on a new importance.

Oganessian has indicated that the large cross sections for SHE production in ^{48}Ca reactions with actinide targets result from enhanced survivability of the compound nucleus during de-excitation by neutron evaporation in competition with fission [2]. Spherical shell effects expected in the region approaching Z=114 and N=184 should lead to larger fission barriers, which could be expected to result in enhanced survival of the heavy element products. However, compared to the trend of exponentially decreasing cross sections with increasing Z (see fig. 11 of [2]), up to six orders of magnitude of cross section enhancement during evaporation of four neutrons is required to explain the picobarn-level SHE cross sections. It should be noted that a similar enhancement of the compound nucleus evaporation residue (EVR) cross sections was not observed [6] in the vicinity of the strong spherical N=126 shell.

We have undertaken a systematic study of heavy element formation by compound nucleus – evaporation reactions using ^{238}U targets with neutron-rich projectiles from ^{22}Ne through ^{37}Cl to provide data for understanding and modeling these reactions. Together with data from similar reactions with ^{18}O [7], ^{19}F [7], ^{34}S [8], ^{40}Ar [9], and ^{48}Ca [5,10-14], cross section trends are analyzed to arrive at conclusions about critical angular momentum for fusion (l_{crit}), survival during deexcitation by neutron evaporation in competition with fission and other de-excitation modes (Γ_n/Γ_{tot}), comparisons with the standard fusion-evaporation model HIVAP [15], and extrapolation to SHE cross sections.

The LBNL 88-Inch Cyclotron accelerated beams of ^{22}Ne, ^{23}Na, ^{26}Mg, ^{27}Al, ^{30}Si, ^{31}P, and ^{37}Cl to selected energies (Table I). Products of compound nucleus reactions were separated from beam and other reaction products with the Berkeley Gas-filled Separator (BGS) [12,13,16]. Targets were prepared by evaporation of UF_4 onto arc-shaped Al or C backing foils. UF_4 target segments were arranged on the periphery of a 35-cm diameter target wheel located 1 cm downstream of a carbon entrance window. To prevent local overheating of the targets, the wheel was rotated at ~ 10 Hz. The product of beam intensity and target thickness was monitored by detecting Rutherford-scattered projectiles with two Si *p-i-n* diode "monitor detectors" mounted at ±27º from the beam axis. Beam energies in the UF_4 target layer were calculated by the residual range technique with range values taken from SRIM2003 [17]. Compound nucleus excitation energies, E^*, were calculated using experimental mass defects for the projectile and target, together with Thomas-Fermi mass defects [18,19] for compound nuclei.

Compound nucleus EVRs are formed with the momentum of the projectile and recoil from the target. The BGS separates EVRs from beam and other reaction products by their differing magnetic rigidities in 66-Pa He gas. Magnetic rigidities for EVRs were estimated as in previous work [13], with an additional correction for higher average EVR charge states observed for low-velocity EVRs in He. The efficiency, ε_{BGS}, for collecting EVRs at the BGS focal plane detector was estimated using a Monte Carlo simulation of EVR trajectories in the BGS, as described earlier [12,16] (Table I).

Details of the Si-strip detector array and data acquisition system are as reported earlier [13,20]. However, because of the short range expected for EVRs from these asymmetric reactions, no multiwire proportional counter was used with beams lighter than ^{37}Cl.

For ^{238}U(^{22}Ne,xn)$^{260\text{-}x}$No, ^{238}U(^{23}Na,xn)$^{261\text{-}x}$Lr, and portions of the ^{238}U(^{26}Mg,xn)$^{264\text{-}x}$Rf irradiations, the beam was chopped at a 50% duty factor with a period of 600 ms. $^{254\text{-}256}$No were identified in α-decay singles spectra recorded between beam pulses. $^{255\text{-}257}$Lr and ^{259}Rf were identified using EVR-α correlations (EVR during beam pulse, α between beam pulses). All other irradiations were carried out with a DC beam. ^{258,260}Rf and ^{262,264}Sg were identified by EVR-SF correlations. To measure α decay of ^{261}Rf, $^{259\text{-}261}$Db, ^{263}Sg, and to search for α-decay of ^{264}Bh and ^{270,271}Mt, a fast beam shutoff mode was used. Upon detection of a potential EVR followed by a time- and position- correlated parent α-decay candidate, the beam was switched off for a preset time to allow a search for α- and SF-decays of the daughters under greatly reduced background conditions. Cross sections are presented in Table I. Error limits represent 68% statistical confidence limits calculated by a Poisson technique [21]. Results for the ^{238}U(^{30}Si,xn)$^{268\text{-}x}$Sg reaction have been reported earlier [22].

Excitation functions for EVR cross sections measured in this work are presented in Fig. 1. The curves in Fig. 1 are fits using a Gaussian smoothly joined to an exponential on the high-energy side,

$$\begin{aligned} &\sigma = \sigma_{\max} e^{-(E^*-c)^2/2w^2}, \; E^* \le \lambda w^2 + c \\ &\sigma = \sigma_{\max} e^{\lambda^2 w^2/2} e^{-\lambda(E^*-c)}, \; E^* > \lambda w^2 + c \end{aligned} \qquad (1)$$

where σ_{max} is the amplitude of a Gaussian with centroid, c, and width, w, $-\lambda$ is the exponential slope, and E^* is the excitation energy. For all target-projectile pairs, w was fixed at 2.8, 3.3, and 3.8 MeV, and λ was fixed at 0.48, 0.38, and 0.28 MeV^{-1} for the 4n, 5n, and 6n exit channels, respectively, to empirically match the excitation function shapes. The centroids and amplitudes of the fits for reactions with even-Z projectiles are listed in Table II. The ^{238}U(^{22}Ne,xn)$^{260\text{-}x}$No excitation functions from this work agree with published results [7], once the laboratory-frame beam energies from the earlier work are adjusted by -4 MeV. This gives us confidence to include data from their ^{238}U(^{18}O,xn)$^{256\text{-}x}$Fm and ^{238}U(^{19}F,xn)$^{257\text{-}x}$Md experiments in our analysis of cross section systematics. Peak cross sections (σ_{max}) for 4n, 5n, and 6n exit channels, together with some tentative 3n cross sections, for various projectiles with ^{238}U targets are plotted in Fig. 2 as a function of the fusing system effective fissility [25]. Also included in Fig. 2 are data from experiments with heavier projectiles [8,9], including a point for the ^{238}U(^{48}Ca,3n)^{283}112 cross section resulting from a meta-analysis of results from several experiments [5,10-14]. The heavy straight lines are exponential fits to peak cross sections for even-Z projectiles. Examination of Table II and Fig. 2 shows that the exponential fits to the 4n, 5n, and 6n excitation function peaks are nearly parallel. The 5n exit channels have the largest σ_{max}, peaking near E^* = 49.5 MeV. The 6n exit channels peak near E^* = 56.1 MeV, with σ_{max} ~ 0.4 of the maxima of the respective 5n exit channels. The 4n exit channels peak near E^* = 41.9 MeV with σ_{max} ~ 0.2 of the maxima of the respective 5n exit channels. The σ_{max} for reactions with odd-Z projectiles are lower than the trends indicated by the heavy lines through the σ_{max} of the even-Z cross sections because the odd-Z reactions occur at energies approximately 5 MeV further below the barrier than those with even-Z projectiles. This is illustrated by the relative positions of reaction thresholds and barriers in Fig. 1. Also included in Fig. 2 are the excitation function peaks as calculated with the standard fusion-evaporation code, HIVAP [15]. HIVAP correctly predicts a) approximate excitation function peak cross sections, b) cross section trends with increasing compound-nucleus Z, and c) the magnitude of odd-even effects.

Formation cross sections for EVRs , σ_{EVR}, in heavy element compound nucleus reactions can be described as

$$\sigma_{EVR} = \sigma_{cap} \cdot P_{CN} \cdot P_x \cdot \prod_{i=1}^{x} \left(\Gamma_n / \Gamma_{tot}\right)_i \quad , \tag{2}$$

where σ_{cap} is the capture cross section, P_{CN} is the compound nucleus formation probability after capture occurs, and P_x is the probability for emitting exactly x neutrons. All terms are functions of Z, A, and E^*. Using relation (2) to calculate a cross section ratio for reactions differing by a single neutron in the exit channel, and solving for first-stage Γ_n/Γ_{tot} in the reaction resulting from emission of the larger number of neutrons gives

$$\Gamma_n/\Gamma_{tot}(A,E_1) = \frac{\sigma_{EVR}(A-x,E_1)}{\sigma_{EVR}(A-x+1,E_2)} \cdot \frac{\sigma_{cap}(A,E_2)}{\sigma_{cap}(A,E_1)} \cdot \frac{P_{CN}(A,E_2)}{P_{CN}(A,E_1)} \cdot \frac{P_{x-1}(A,E_2)}{P_x(A,E_1)} \cdot \prod_{i=2}^{x} \left(\frac{\Gamma_n/\Gamma_{tot}(A-i+2,E_i)}{\Gamma_n/\Gamma_{tot}(A-i+1,E_i)} \right) \tag{3}.$$

Here A is the compound nucleus mass number. E_1 is the excitation energy of the compound nucleus for the $\sigma_{EVR}(A\text{-}x,E_1)$ reaction. E_2 is the resulting excitation energy in the A-1 product after neutron emission. The $\sigma_{EVR}(A\text{-}x\text{+}1,E_2)$ is chosen at E_2 to closely match the excitation energies in the subsequent neutron evaporation cascades. E_2 through E_x in the product term are identical for both members of the reaction pair. $\sigma_{EVR}(A\text{-}x,E_1)/\sigma_{EVR}(A\text{-}x\text{-}1,E_2)$ are determined from the fits to the excitation functions (Fig. 1, Table II). $\sigma_{cap}(A,E_2)/\sigma_{cap}(A,E_1)$ have been calculated using the approximate "barrier distribution" scheme of Świątecki, Siwek-Wilczyńska and Wilczyński [26] with updated parameters [27]. $P_{CN}(A,E_2)/P_{CN}(A,E_1)$ have been assumed to be 1. P_x have been calculated according to the formalism summarized by Vandenbosch and Huizenga [28]. E_i were chosen so that successive values differ by the sum of the appropriate neutron separation energy and an average neutron kinetic energy. In addition, E_5 were chosen to match the peaks of the 5n excitation functions, ensuring that $P_{4\text{-}6}$ are large, and $P_{x\text{-}1}(A,E_2)/P_x(A,E_1)$ are near 1. Sikkeland, Ghiorso, and Nurmia [29] have made an

E^*-independent empirical fit to the geometric mean of the Γ_n/Γ_f for several stages of neutron evaporation as a function of Z and average N of the neutron cascade for Z=98-104. For all de-excitation cascades considered in this work, this results in

$$\Gamma_n/\Gamma_{tot}(A+1) \,/\, \Gamma_n/\Gamma_{tot}(A) = 1.12 \qquad (4)$$

which has been applied inside the product term at the end of equation (3). The resulting E_1 and $\Gamma_n/\Gamma_{tot}(A,E_1)$ appear in the last two columns of Table II. The first-stage Γ_n/Γ_{tot} values for the 5n excitation energies show a weak dependence on compound nucleus Z and have large values, similar to those reported by Andreyev [30]. However, use of an energy-dependent P_{CN} could result in $P_{CN}(A\text{-}1,E_2)/P_{CN}(A,E_1) < 1$, and correspondingly smaller first-stage Γ_n/Γ_{tot} values for the *5n* excitation energies. For each entry in Table II, the capture cross section, σ_{cap}, has been calculated [26,27]. The maximum angular momenta, l_{max}, associated with these capture cross sections are listed. The fact that the amplitudes of the 5n excitation functions are larger than those for the 4n exit channels shows that l_{crit} does not limit fusion at energies up to the centroids of the 5n channels, with l_{max} = 26-33 $\hbar$. The smaller first-stage Γ_n/Γ_{tot} at the 6n excitation energies for ^{26}Mg + ^{238}U and ^{30}Si + ^{238}U are unexpected. Assuming l_{crit} values slightly larger than l_{max} = 26-33 $\hbar$ would result in larger values for first-stage Γ_n/Γ_{tot} than listed at the 6n excitation energies in Table II. l_{crit} values of > 33 $\hbar$ [31] and 40-49 $\hbar$ [32] have been reported for production of Z=102-107 isotopes in more symmetric reactions with Tl-Bi targets.

Cross sections for heavy element formation in reactions with heavy ions and ^{238}U targets decrease exponentially with increasing Z or effective fissility. The point for the ^{238}U(^{48}Ca,3n)^{283}112 reaction in Fig. 2 lies two orders of magnitude above the exponential trend. Reported picobarn-level SHE cross sections for all other reactions [2] between ^{48}Ca projectiles and actinide targets (with effective fissilities as large as 0.899) are as much as 5 orders of magnitude above the respective Fig. 2 trend lines. An enhanced understanding of Γ_n/Γ_{tot} and/or P_{CN} is needed to explain SHE cross sections. Future experiments with more neutron-deficient projectiles can obtain more accurate values for Γ_n/Γ_{tot} by forcing the product term in equation (3) to 1, and eliminating the need for use of the equation (4) approximation.

We gratefully acknowledge the operations staff of the 88-Inch Cyclotron for providing stable, high-intensity beams. Some ^{238}U targets and carbon foil entrance windows were produced by the target lab at the Gesellschaft für Schwerionenforschung. Financial support was provided by the Office of High Energy and Nuclear Physics, Nuclear Physics Division of the U.S. Department of Energy, under contract DE-AC02-05CH11231.

---

[1] P. Armbruster, Acta Phys. Pol. B **34**, 1825 (2003).

[2] Y. Oganessian, J. Phys. G **34**, R165 (2007).

[3] S. Hofmann, Rep. Prog. Phys. **61**, 639 (1998).

[4] R. Eichler *et al*., Nucl. Phys. A **787**, 373c (2007).

[5] S. Hofmann *et al*., Eur. Phys. J. A **32**, 251 (2007).

[6] D. Vermeulen *et al*., Z. Phys. **318**, 157 (1984).

[7] E. D. Donets, V. A. Shchegolev, and V. A. Ermakov, Sov. J. Nucl. Phys. **2**, 723 (1966).

[8] Yu. A. Lazarev *et al*., Phys. Rev. Lett. **75**, 1903 (1995).

[9] S. Hofmann, private communication (2003).

[10] Yu.Ts. Oganessian *et al.*, Eur. Phys. J. A **5**, 63 (1999).

[11] Yu.Ts. Oganessian *et al.*, Eur. Phys. J. A **19**, 3 (2004).

[12] W. Loveland *et al*., Phys. Rev. C **66**, 044617 (2002).

[13] K. E. Gregorich *et al.*, Phys. Rev. C **72**, 014605 (2005).

[14] Yu.Ts. Oganessian *et al.*, Phys. Rev. C **70**, 064609 (2004).

[15] W. Reisdorf, and M. Schädel, Z. Phys. A **343**, 47 (1992).

[16] K. E. Gregorich *et al.*, Eur. Phys. J. A **18**, 633 (2003).

[17] J. F. Ziegler, Nucl. Instrum. Methods Phys. Res. B **219-220**, 1027 (2004).

[18] W. D. Myers and W. J. Swiatecki, Nucl. Phys. A **601**, 141 (1996).

[19] W. D. Myers and W. J. Swiatecki, (Lawrence Berkeley National Laboratory Report LBNL-36803, 1994).

[20] C. M. Folden III *et al.*, Phys. Rev. Lett. **93**, 212702 (2004).

[21] K.-H. Schmidt, *et al*., Z. Phys. A **316**, 19 (1984).

[22] K. E. Gregorich *et al*., Phys. Rev. C **74**, 044611 (2006).

[23] I. Ahmad *et al*., Phys. Rev. C **17**, 2163 (1978).

[24] K. Nishio *et al*., Eur. Phys. J. A **29**, 281 (2006).

[25] J. Blocki, H. Feldmeyer, and W. J. Świątecki, Nucl. Phys. **A459**, 145 (1986).

[26] W. J. Świątecki, K. Siwek-Wilczyńska, and J. Wilczyński, Phys. Rev. C **71**, 014602 (2005).

[27] K. Siwek-Wilczyńska, and J. Wilczyński, private communication (2006).

[28] R. Vandenbosch, and J. R. Huizenga, *Nuclear fission*, Academic Press, New York, (1973) p. 224.

[29] T. Sikkeland, A. Ghiorso, and M. J. Nurmia, Phys. Rev. **172**, 1232 (1968).

[30] A.N. Andreyev, *Heavy-ion fusion: exploring the variety of nuclear properties*, World Scientific, Singapore (1994) p260.

[31] T. L. Khoo, *et al*., Argonne Nat. Lab. Report ANL-06/53, p23 (2006).

[32] M.T. Magda, *et al*., J. Phys. G **6**, 221 (1980).

Table I. Cross sections for ^{238}U(HI,xn) reactions.

E^* (MeV)	ε_{BGS}	4n (pb)	5n (pb)	6n (pb)
^{22}Ne + ^{238}U[a]		^{256}No	^{255}No	^{254}No
34.4(2)	0.19	2700(1400)		
37.2(2)	0.19	16000(3000)		
39.9(2)	0.20	15000(4000)	<3000	
45.0(2)	0.22	10000(3000)	76000(15000)	
50.0(2)	0.24	<1900	70000(14000)	<8600
55.1(2)	0.26		21000(6000)	28000(8000)
^{23}Na + ^{238}U[a]		^{257}Lr	^{256,255}Lr	
39.9(2)	0.24	190^{+430}_{-160}	1300^{+700}_{-500}	
44.9(2)	0.26	470^{+1070}_{-390}	3300^{+1800}_{-1200}	
49.9(3)	0.28	200^{+440}_{-160}	5300^{+1200}_{-1000}	
^{26}Mg + ^{238}U[b]		^{260}Rf	^{259}Rf	^{258}Rf
35.3(9)	0.15	50^{+18}_{-14}		
41.0(9)	0.16	170^{+80}_{-60}	<120	
45.4(9)	0.18	180^{+80}_{-60}	440^{+300}_{-190}	
50.4(13)	0.19		1560^{+460}_{-360}	250^{+120}_{-90}
55.8(9)	0.21		380^{+360}_{-200}	770^{+200}_{-180}
62.0(9)	0.22		190^{+240}_{-120}	430^{+130}_{-110}
^{27}Al + ^{238}U[b]		^{261}Db	^{260}Db	^{259}Db
40.5(10)	0.19	20^{+45}_{-16}		
45.6(10)	0.20	57^{+75}_{-37}	<45	<45
50.6(10)	0.21	<32	53^{+51}_{-29}	18^{+40}_{-15}
^{30}Si + ^{238}U[b]		^{264}Sg	^{263}Sg	^{262}Sg
39.3(20)	0.27	10^{+7}_{-4}	<9.0	
44.8(11)	0.29	<8.6	18^{+33}_{-12}	<8.6
53.7(20)	0.32		54^{+31}_{-23}	27^{+12}_{-9}
60.8(11)	0.36		$2.6^{+5.9}_{-2.1}$	15^{+9}_{-6}
^{31}P + ^{238}U[b]		^{265}Bh	^{264}Bh	^{263}Bh
50.1(12)	0.35		<4.5(α) $\leq 1.9^{+2.5}_{-1.2}$ (SF)[d]	
^{37}Cl + ^{238}U[c]		^{271}Mt	^{270}Mt	^{269}Mt
47.3(15)	0.40	<1.1(α) ≤0.7(SF)	<1.1(α) ≤0.7(SF)	

[a] Targets were 160 μg/cm^2 $^{238}UF_4$ on 40 μg/cm^2 C.
[b] Targets were 470 μg/cm^2 $^{238}UF_4$ on 580 μg/cm^2 Al.
[c] Targets were 660 μg/cm^2 $^{238}UF_4$ on 580 μg/cm^2 Al.
[d] Two EVR-SF events which *may be* Bh were observed.

Table II. Fits to even-Z excitation functions.

x	c MeV	σ_{max}	σ_{cap} mb	l_{max} ħ	E_1 MeV	$\Gamma_n/\Gamma_{tot}(A,E_1)$
$^{238}U(^{18}O,xn)^{256-x}Fm$ [7]						
6	55	1900 nb	540	35	58.8	0.86(24)
5	48	2200 nb[a]	319	26	49.2	0.89(25)
4	43	750 nb	140	16	41.1	<0.87(35)>[b]
3	43[c]	3 nb[c]	140	16		
$^{238}U(^{22}Ne,xn)^{260-x}No$						
6	56.1[d]	27(8) nb	452	38	59.3	0.22(7)
5	48.2(5)	95(13) nb	228	26	49.2	0.64(13)
4	40.0(6)	21(3) nb	25	8	40.7	<0.38(14)>
$^{238}U(^{26}Mg,xn)^{264-x}Rf$						
6	57.0(8)	910(150) pb	399	43	59.6	0.49(14)
5	50.5(9)	1520(350) pb	239	32	49.2	0.71(25)
4	41.1(7)	320(70) pb	33	11	40.4	<0.59(27)>
3	35.5[c]	30^{+60}_{-20} pb[c]	2	2		
$^{238}U(^{30}Si,xn)^{268-x}Sg$						
6	56.0(14)	33(10) pb	325	43	59.8	0.26(16)
5	50.5(16)	82(44) pb	199	33	49.2	1.24(95)
4	41.4[e]	12(7) pb	31	12	40.2	<0.57(56)>
3	39.6[c] [24]	$\leq 3.5^{+8.1}_{-2.9}$ pb[c]	16	8		

[a] Published cross section (assumed I_α = 1% [7]) corrected for I_α = 1.8% [23].
[b] Geometric mean of Γ_n/Γ_{tot} at x = 5, 6.
[c] Cross section measured at a single energy.
[d] Fixed at average of the other 6*n* centroids.
[e] Fixed at average of the other 4*n* centroids.

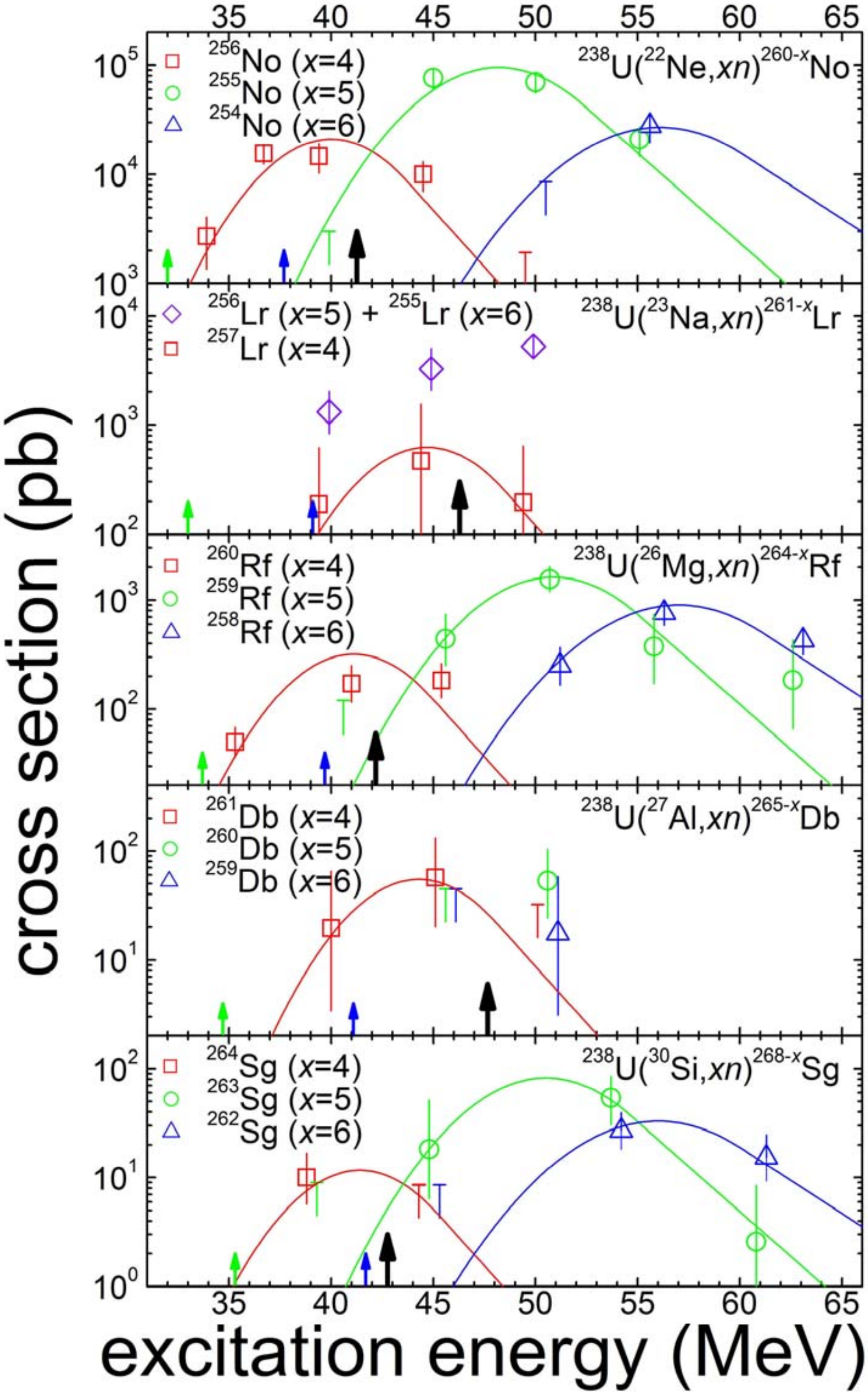

FIG. 1. (Color online) Experimental cross sections. 4*n*, 5*n*, and 6*n* exit channels are designated by squares, circles and triangles, respectively. The curves are fits as explained in the text. Large arrows indicate interaction barriers [26,27]. Small arrows show 5*n* and 6*n* threshold energies.

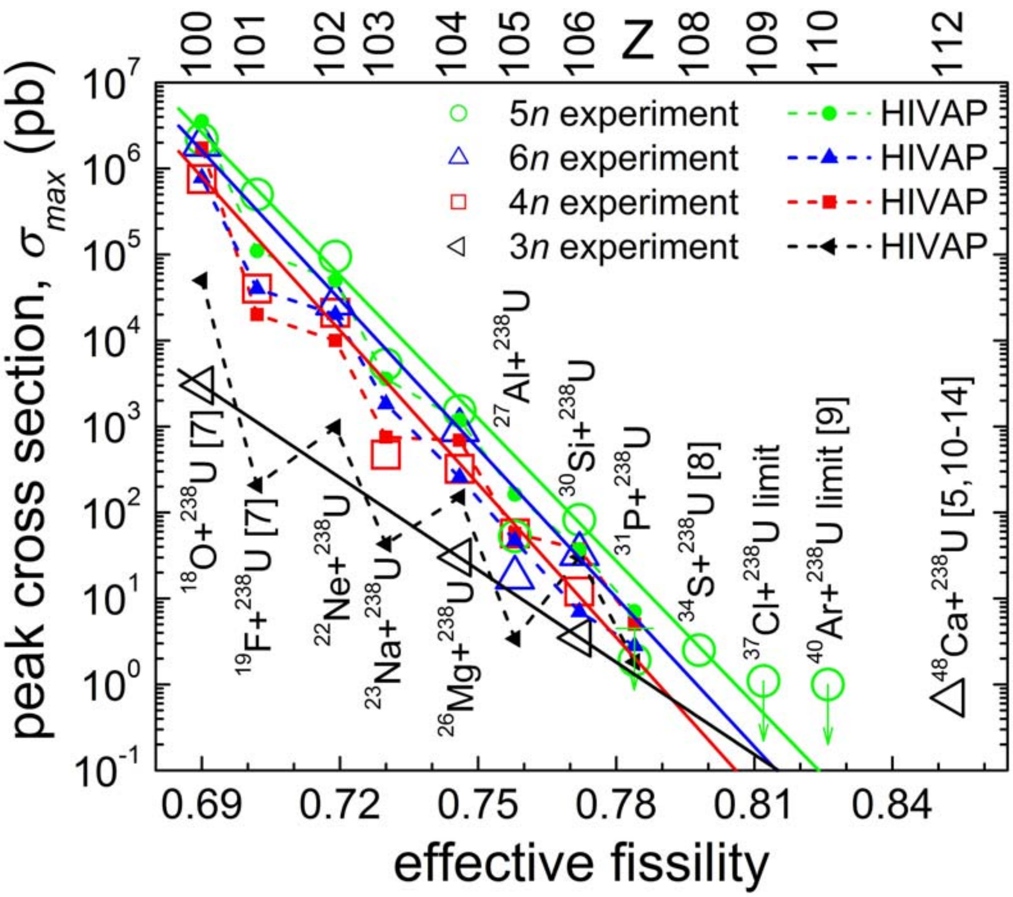

FIG. 2. (Color online) σ_{max} (open symbols) as a function of effective fissility [25]. Heavy straight lines (top to bottom) are exponential fits to even-Z σ_{max} for the 5n, 6n, 4n, and 3n exit channels. Filled symbols connected by dahsed lines are results of HIVAP calculations [15].